Comparison of electromagnetic inspection methods for creep-degraded high chromium ferritic steels

Bhaawan Gupta, Benjamin Ducharne, Tetsuya Uchimoto, Gael Sebald, Takamichi Miyazaki, Toshiyuki Takagi

Comparison of electromagnetic inspection methods for creep-degraded high chromium ferritic steels.

Bhaawan Gupta[a,b,c], Benjamin Ducharne[b], Tetsuya Uchimoto[a,b], Gael Sebald[a], Takamichi Miyazaki[d], Toshiyuki Takagi[a,c]*

[a]ELyTMaX UMI 3757, CNRS – Université de Lyon – Tohoku University, International Joint Unit, Tohoku University, Sendai, Japan

[b]Univ Lyon, INSA-Lyon, LGEF, EA682, F-69621, Villeurbanne, France

[c]Institute of Fluid Science, Tohoku University, Sendai, Japan

[d]Instrumental Analysis Group, Graduate School of Engineering, Tohoku University, Sendai, Japan

Corresponding Authors

**E-mail: benjamin.ducharne@insa-lyon.fr*

Abstract

Nondestructive testing (NDT) techniques are used to evaluate the material degradation of ferromagnetic materials, for example, in sensitive environments, such as thermal power plants, where the materials are subjected to creep damage. There is no consensus on the use of an electromagnetic NDT technique to characterize the evolution of creep damage in high-chromium ferritic steels. In this work, an overview and comparison of three different electromagnetic NDT techniques that were applied to high-chromium steels is provided to understand creep evolution in terms of microstructural changes, such as precipitation, dislocation and grain size. To quantify the empirical measurements, a modeling technique was proposed for each applied method. The model parameters were optimized for each NDT technique and tested material. Depending on the model parameters, the accuracy of the parameter determination depends strongly on the NDT technique, which indicates its correlation with the microstructural information.

Keywords

Electromagnetic NonDestructive Testing, Micromagnetic Modeling, High-Chromium Steel, Creep Degradation, Jiles–Atherton Model.

1. Introduction

1.1. General introduction

In thermal power plants, materials that are used in turbines and boilers are exposed to high temperatures and pressures [1][2]. This continuous exposure can lead to microstructural changes in the materials which, if not monitored in good time, can lead to serious and catastrophic incidents. Normally, all NDT techniques aim to identify physical material damage, which appears at a later stage. After crack initiation, the crack length grows exponentially and, in most cases, it becomes too late to avoid damage and consequently, an incident. It can be assumed that before the crack appears, the materials undergo microstructural changes, which, if monitored continuously, can help to avoid unwanted incidents. The concept of crack length versus time is shown in Fig. 1 [3]. To monitor microstructural changes, imaging techniques, such as scanning electron microscopy (SEM) and electron backscatter diffraction (EBSD) can be used to provide access to microscopic material information [4]. To analyze the materials using such techniques, the material must be of a specific shape and size and requires extensive sample preparation effort that is beyond the scope of NDT.

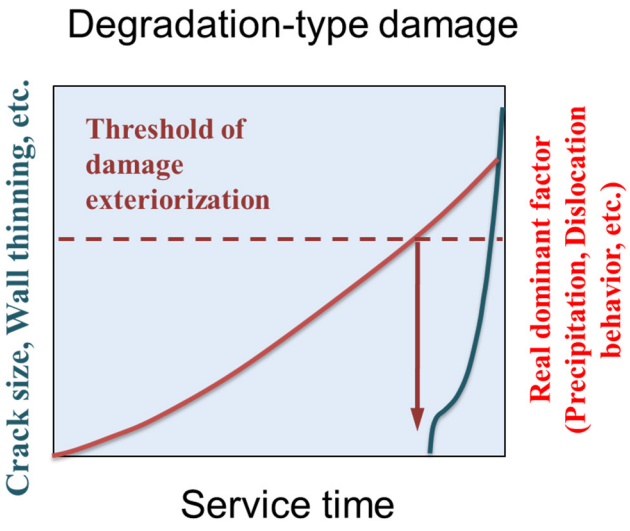

Figure 1: Concept of crack length versus service time for degradation-type flaws.

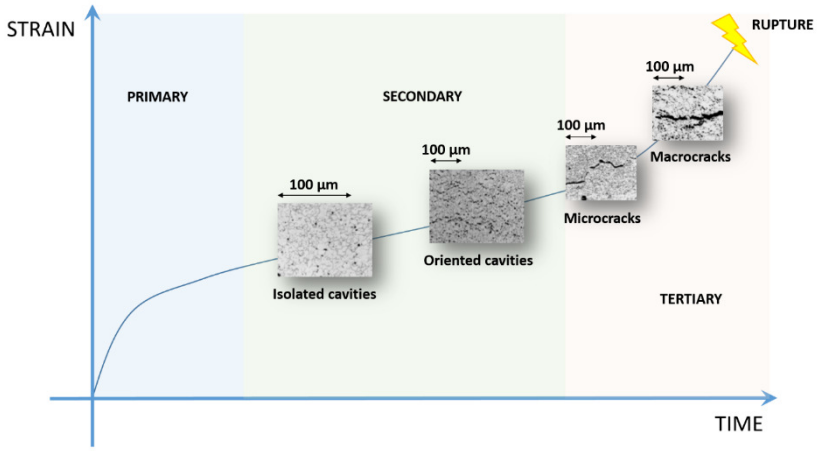

Figure 2: Strain versus time variations for a sample under creep degradation.

Such techniques are useful at the laboratory scale but in in-situ applications, the required equipment is not portable and applicable to derive microstructural information. Fig. 2 shows the evolution of creep in materials at the microstructural level on the strain-versus-time graph [5]. Initially, isolated cavities are formed, which eventually grow and form oriented cavities. With further strain application, oriented cavities result in crack formation and material rupture. To access this level of information without using SEM or EBSD, the potential solution is to use magnetic signatures and correlate these to the material microstructure.

Local interactions provide a magnetic signature to the ferromagnetic materials, because the magnetic response has a strong dependence on the microstructure composition and distribution. Magnetic measurements are sensitive to the time evolution of microstructures, which makes them a sensitive tool for the nondestructive testing of creep degradation. From a creep perspective, several techniques have been studied, mostly on low-alloy steel with no correlation as shown in Table 1 [1]. Selectivity defines the choice and effectiveness of the technique. Contradictory information can be found in the literature about the selectivity of

the magnetic controls. On a one hand, Sposito et al. classify the selectivity as poor, on the other hand Tomas et al. results indicate reliable applicability to detect early stages of the material fatigue, and to predict its residual lifetime [1][6]. NDT techniques for high-chromium steels have not yet been established.

Tab 1: Comparison of NDT methods.

Technique	Sensitivity	Selectivity	Damage Type
Replication	Surface only	++	Localized
Ultrasonic	Average over thickness	++(Later stages) Surface sensitive	Localized / Volumetric
Magnetic Properties	Bulk	-/+	Volumetric
Barkhausen Emission	Thin sub-surface layers	+ (Surface sensitive)	Localized
Eddy current	Decays rapidly with depth	--	Volumetric

++ Good
-- Poor

Ferromagnetic materials are characterized by strong internal magnetic interactions. Equilibrium is reached by minimizing energies (exchange energy, anisotropy energy, magneto-elastic energy, magneto static energy) [7]-[9]. The distortion of magnetic domain distribution under the influence of an external magnetic field is not a smooth process. The domain wall movements are strongly stochastic; they correspond to strain, oscillations and jumps over pining sites (grain boundaries, interfaces, inclusions, precipitates, dislocations). The microstructural defects act as local energy barriers to prevent easy magnetization and

create time delays between the magnetic excitation and magnetization of the ferromagnetic sample.

1.2. Tested specimens

High-chromium ferritic steel (12% chromium steel) is used commonly for high-temperature power plant components, such as steam turbine rotor blades and gas turbine compressor blades [10]. Chromium is used frequently to increase the resistance to corrosion and erosion. Ten samples of high-chromium ferritic steels from the same batch were aged under incremental conditions of temperature and stress as shown in Table 2.

Tab 2: Aged high-chromium steel samples.

Sample number	Stress [MPa]	Temp [°C]	Test time [h]
0	0	0	0.0
1	343	550	281.8
2	343	550	785.6
3	343	550	2205.7
4	201	600	255.6
5	201	600	763.9
6	201	600	1725.9
7	98	650	256.3
8	98	650	789.6
9	98	650	1736.8

The aim of the aging process is to reproduce the working conditions and to observe the microstructural variations at different levels of degradation. To maintain the rupture time from three different categories of temperature-treated samples as constant as possible, the stress was adapted to different values. Prior to the magnetic investigation, 10 samples were subjected to a fine microstructural analysis. SEM imaging followed by EBSD was performed on the sample cross-sectional surface [11]. From these images, a set of four parameters were collected: the Kernel average misorientation (KAM) coefficient, the hardness, the grain size and the precipitation number. Sample geometrical information are depicted in Fig. 3 below:

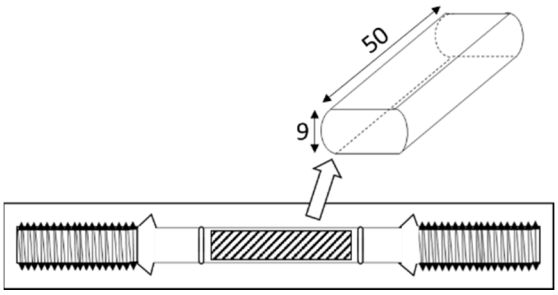

Figure 3: Sample geometrical information.

1.3. Manuscript structure

Three magnetic properties were compared: the magnetic hysteresis curve B(H), the magnetic incremental permeability (MIP) and the magnetic Barkhausen noise (MBN). The microstructural information was correlated with the magnetic parameters that had been derived using different techniques, as described in Section 2. To unify the different NDT techniques, the Jiles–Atherton (J–A) model was adapted to simulate each NDT technique, where model parameters were derived from NDT measurements only as detailed in Section 3. In Section 4, the accuracy of the model parameters for each NDT technique, and their correlation to microstructure is discussed.

2. Magnetic characterization

The magnetic signature of a ferromagnetic material is dependent on the microstructural properties. The dependency is complex and not linear. Standard characterization of the magnetic properties converges toward experimental situations where the observed magnetic state and the magnetic excitation are in the same direction and orientation. This is the case of the Epstein Frame [12], the single sheet tester [13]-[14] or the ring-shape-type standard characterization [15]. The hysteresis cycles that are obtained under such experimental conditions are particularly useful as they provide access to the classic magnetic absolute

indicators (the remanent induction, coercivity, differential permeability, hysteresis area and even the frequency dependence) [16]. Unfortunately, the working conditions and geometries of structural steels, such as those tested in this study are far from the ideal experimental situation that is described in standard characterization norms. Sharp and oversize shapes forbid the use of surrounding coils and access to a magnetic flux that is confined inside crossed areas where an average induction field *B* could be determined. Alternative instrumentation and indicators of the magnetic state must be proposed to address this issue. In this study, three different magnetic experimental situations were explored to monitor the largest possible number of magnetic indicators and establish which was most sensitive to creep damage. Even if the use of surrounding coils is mostly incompatible with the industrial exploitation of high-chromium steels, the need for reliable and standard experimental results implies that our measuring starts with classic *B(H)* hysteresis cycles.

2.1 Magnetic hysteresis cycle

Major hysteresis cycle *B(H)* may be considered a reference magnetic inspection method. Numerous work has claimed that much information can be obtained by analyzing the shape and orientation of the hysteresis loop for a tested material [17]. However, hysteresis provides global and not local sample information. Hence, some information that may affect creep at the microstructural level may be omitted. Standardization of B(H) measurements exist already (VSM, Epstein frame, ring specimen [12][18][19]), but for these methods, the sample must be of a specific dimension, which limits the applicability of this technique to the field of NDT and real-time situations. Furthermore, even if one wants to measure the instantaneous sample magnetic response, the sample must be surrounded by coils to record the induced

voltage that corresponds to the induced magnetic flux density (B). Coil introduction around the sample limits this hysteresis measurement inspection method for inclusion in NDT.

In this experimental setup, samples were surrounded by 50 turns of coil, which is sufficient to measure a well-defined electromotive force. The sample is magnetically excited with a sinusoidal external magnetic field H, of 10^4 A/m maximum amplitude, and is frequency limited to 0.1 Hz to avoid dynamical effects. A U-shaped Yoke is used to drive the magnetic excitation to the tested samples. Because the surrounding coil measures the induced voltage, B is calculated from:

$$B(t) = -\frac{1}{n.S}.\int_0^t e(t).dt \quad (1)$$

The time variation of the surface tangent magnetic excitation *H*(t) is measured directly using a Hall-effect sensor.

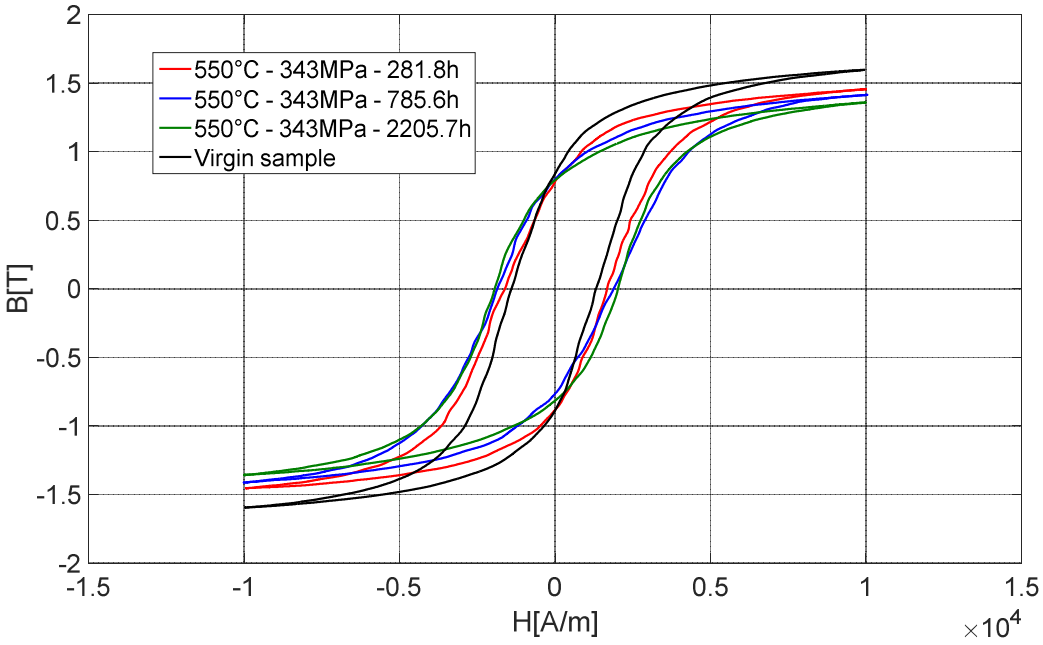

Figure 4: B(H) hysteresis cycles obtained under constant creep conditions with incremental aging time.

In Fig. 4, hysteresis cycles from the same category of materials are plotted with different ageing times. However, differences between samples are not limited within ±15% for the saturated and remnant induction field, or coercive field, for example. This may occur because, with the surrounding coils, extensive information is averaged, which leads to a loss of specific information. In addition, the B(H) curve integrates all contributions of magnetism, domain wall motion and magnetic moment rotation. There is a possibility that some phenomena compensate each other, which minimizes the differences between samples. Hence, as a next step, the Barkhausen noise was evaluated, which is known for its sensitivity to mechanical and microstructural changes.

2.2 Magnetic Barkhausen noise

The Barkhausen noise is sensitive to mechanical changes and to residual stresses [20]-[22]. It can be assumed that mechanical changes in the materials lead to microstructural changes and modifications of the magnetic behavior. These microstructural changes modify the domain wall movements, which makes the Barkhausen noise an interesting technique to study creep phenomenon. The application of micromagnetic NDTs, such as measuring the magnetic Barkhausen noise (MBN), has increased extensively in the industrial field recently [22]. This occurs mainly because of the improvement in signal processing techniques that have enabled and simplified online production monitoring [23]. However, industrial development is limited because of the reproducibility of a raw signal (which comprises high-orders filters and huge gain amplifier stages), and because the results are highly equipment/supplier dependent. To address this issue, some groups have been using the envelope [24][25] or the RMS value of the Barkhausen noise [26] but there is no direct physical meaning of both indicators. The magnetic Barkhausen noise energy (MBN_{energy}) can be used to reconstitute local hysteresis

cycles from the Barkhausen noise measurement. MBN_{energy} hysteresis cycles are obtained by plotting the time integration of the squared Barkhausen noise multiplied by the excitation field time derivation sign as a function of H, see Eq. (2). Here, Bark(t) is the raw MBN signal. The hysteresis cycles constitute good indicators to understand the magnetization process and the influence of microstructural and mechanical properties [27]. The raw Barkhausen noise signal can be considered as an image of the domain wall speed. By integrating the square of the signal (Eq. 2), the area of the resulting MBN_{energy} hysteresis cycles provides an image of the kinetic energy that is consumed by the domain walls during the magnetization process.

$$MBN_{energy}(H) = \int_0^T sgn\left(\frac{dH}{dt}\right).\left(V_{Barkhausen}\right)^2 .dt(H) \qquad (2)$$

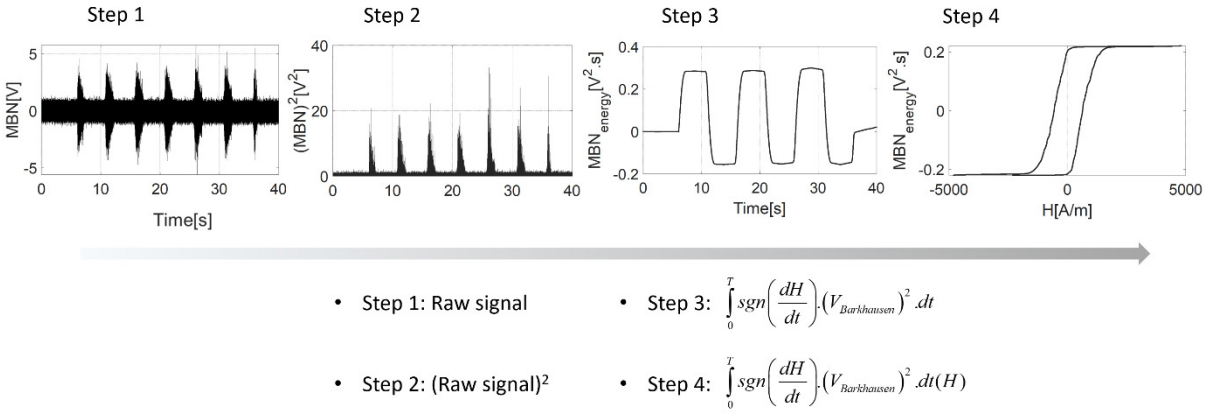

Figure 5: $MBN_{energy}(H)$ hysteresis cycles, plotting process.

An overall illustration, such as a detailed description of the experimental setup to measure the Barkhausen noise signature of our samples, is available in [27]. The magnetic excitation frequency is 0.1 Hz. The skin depth of the MBN measurement can be approximated between 0.01 mm and 0.8 mm. Just the top layer is concerned by this characterization.

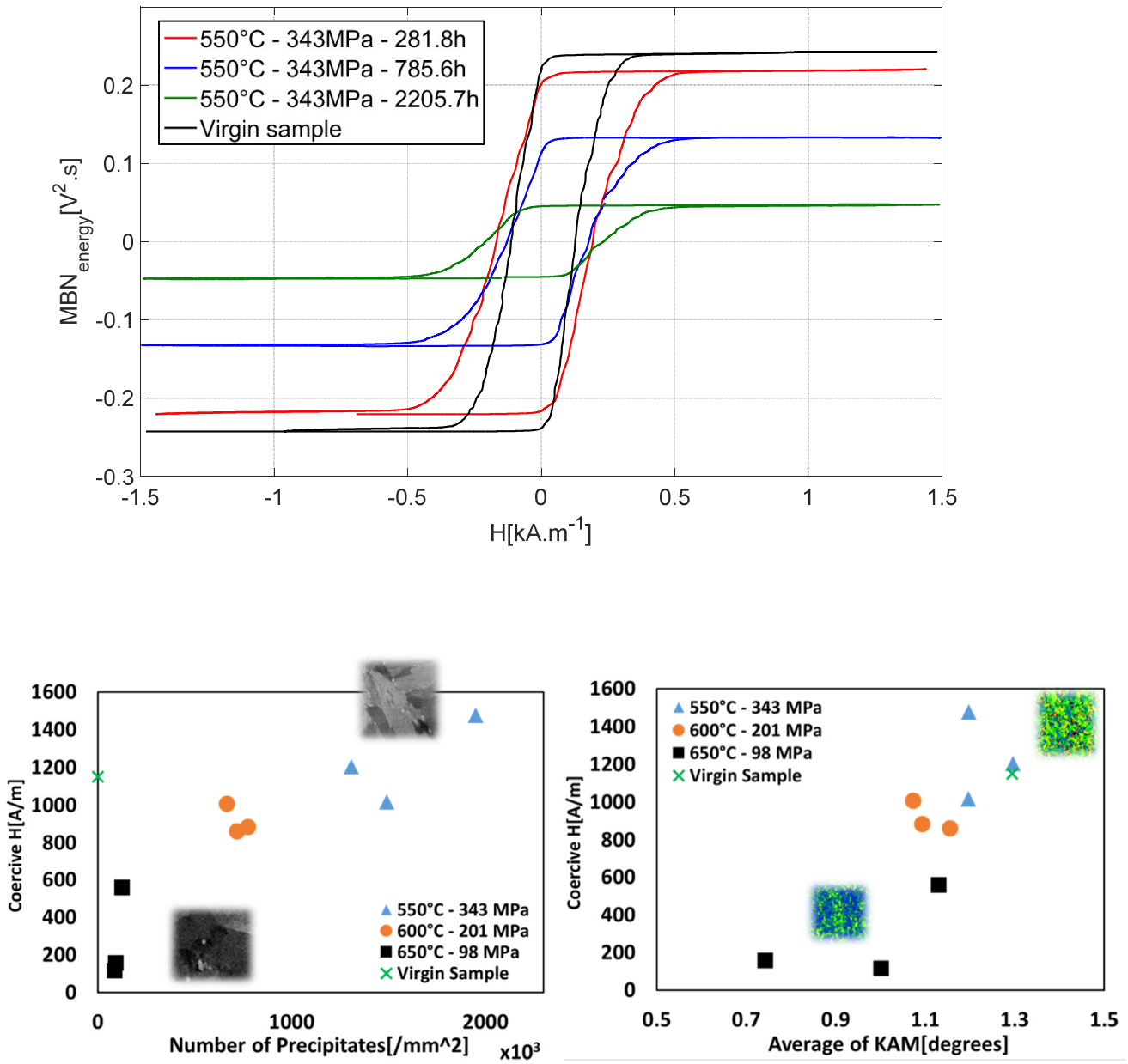

Figure 6: Reconstructed MBNenergy curves and derived parameters from each material temperature category.

Fig. 6 shows the MBN_{energy} curves that were derived from the raw Barkhausen noise signals according to the procedure in Fig. 5. The differences between the same category of materials are stronger compared to the hysteresis cycles in Fig. 4. From these MBN_{energy} curves, parameters such as the coercivity are derived and evaluated against the microstructure. This result implies that materials at a higher temperature become soft magnetic, whereas the

amount of precipitate decreases (with an increase in ageing times). The low-temperature materials tend to harden with an increase in number of precipitates (increase in ageing time). This trend is generic, with some discrepancies, as can be seen in the evaluation graphs in Fig. 6.

2.3 Magnetic Incremental permeability

With exposure to a steady and static magnetic field to a ferromagnetic material, the reversible permeability that is measured with a small alternating magnetic field is defined as the magnetic incremental permeability [28]. Mathematically, the MIP can be defined as [29]:

$$\mu_{\Delta} = \frac{1}{\mu_0} . \frac{\Delta B}{\Delta H} \quad (3)$$

where μ_0, ΔB and ΔH are the air permeability, incremental magnetic flux density and incremental magnetic field, respectively. By measuring the minor loop magnetic flux density during magnetization, the respective magnetic incremental permeability (MIP) can be calculated. The microstructural features in a ferromagnetic material, such as the magnetic domain wall movement, are affected easily by any mechanical damage, such as fatigue damage and plastic deformation. Hence, the MIP method is considered an effective and potential NDT technique to evaluate residual stress and creep [30].

An overall illustration, such as a detailed description of the experimental setup we used to measure the magnetic incremental permeability signature of our samples, is available in [30]. The frequency of the quasi-static magnetic excitation contribution is 0.1 Hz, the frequency of the dynamic magnetic excitation contribution is 50 KHz. The skin depth of the MIP measurement can be approximated between 0.03 mm and 0.125 mm. Just like MBN, just the top layer is concerned by this experimental observation. Fig. 7 compares the similar samples

of hysteresis and MBN_{energy}. Clear distinctions can be made between samples of the same category. The more interesting MIP factor was the correlation between the derived magnetic parameters from these curves and the microstructural information [10]. The MIP showed a stronger correlation. To quantify these results, all three tested techniques were simulated as illustrated in the next section.

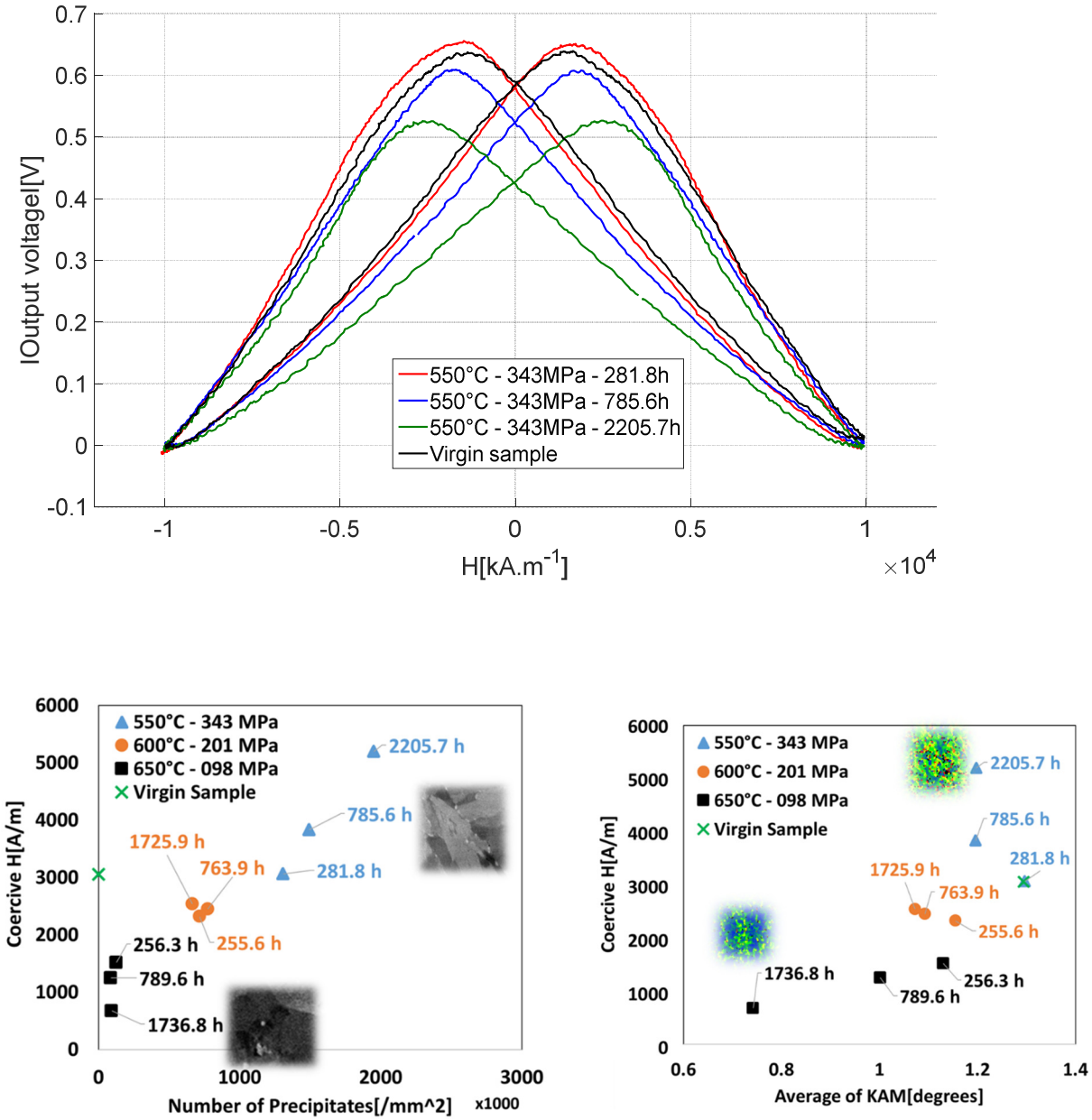

Figure 7: MIP curves for low-temperature category of materials and derived parameters from all samples with respect to microstructure.

Three different magnetic signatures were tested to determine the most sensitive magnetic parameter to creep degradation. As creep degradation is evaluated through microstructural variations, the magnetic parameters are actually plotted as function of these microstructural properties. B(H) characterization is the normalized magnetic standard signature. When it comes to the creep evaluation, it is not the appropriate signature. B conveys average specimen cross section information and the integration step reduces the sensitivity. Among MBN and MIP, It seems complex to pick one method over the other but the following main tendencies can be established:

_ The MIP magnetic parameters are highly sensitive to the precipitation content and to their evolution changes.

_ Concerning grain misorientation, large variations can only be seen on high temperature samples (where the materials tend to become very soft magnetic due to large decrease of dislocations as the rupture level increases).

_ Coercivity read on the MBN_{energy} cycles shows a good correlation in terms of microstructure evolution (precipitation).

_ The amplitude of the MBN_{energy} curves always decreased when the rupture approaches.

3. Simulation tool

The current industrial application of electromagnetic evaluation relies on empirical data obtained on calibration samples under well-known conditions (e.g. stress, hardness). Thresholds of acceptance/rejection and polynomials that represent the target value or databases for pattern recognition are based on these data. At this time, no applicable models are available that would describe the relationship between measured parameters and target material properties. The calibration effort and understanding of the phenomena could be

reduced significantly if such models were known and developed. In this study, a simulation tool was developed to simulate the magnetic characterization situations that were introduced in Section 2.

The objective was to propose a simulation tool based on a limited number of parameters, with a physical meaning and sufficient flexibility to provide correct simulation results under the three experimental situations.

Many ferromagnetic models exist in the literature. Most have been developed to consider the hysteresis constraint in the dimensioning of electromagnetic devices (electric motors, ferromagnetic memories) [31]-[35]. Most models cannot be used in all experimental situations that we want to simulate. Some, such as the Preisach model rely on distribution functions that cannot be interpreted physically [36][37]. Other models, such as the Mel'gui model are limited to the major hysteresis envelop [38].

After multiple investigations, it became clear that because of the strong simulation restrictions that are imposed by the three experimental situations, the only feasible option was to use the J–A based model and adapt it if necessary.

A limited number of parameters and their physical interpretation in the J–A model provides a strong advantage [39][40]. Limitations include its frequency independence, the inter-correlation of parameters and the accommodation issue that can be observed in minor loop situations. For the three magnetic experimental signatures measured in this study, the magnetic excitation frequency is always lower than the quasi-static threshold, thus no dynamical contribution are required in our simulation methods.

3.1 Magnetic hysteresis cycle simulation

The J–A model was developed originally to simulate the magnetic state evolution *M* of a ferromagnetic sample under the influence of a magnetic excitation *H*, and that through a collinearity situation. The richness of the J–A model relies on a limited number of parameters and on a physical justification of the equations and coefficients. According to the J–A theory, the total magnetization *M* can be decomposed into its reversible (M_{rev}) and irreversible (M_{irr}) contribution [41].

The J–A model is particularly well adapted to simulate our magnetic hysteresis experimental situation. The collinear situation is credible and the frequency level of the magnetic excitation is sufficiently low to avoid unconsidered dynamic effects.

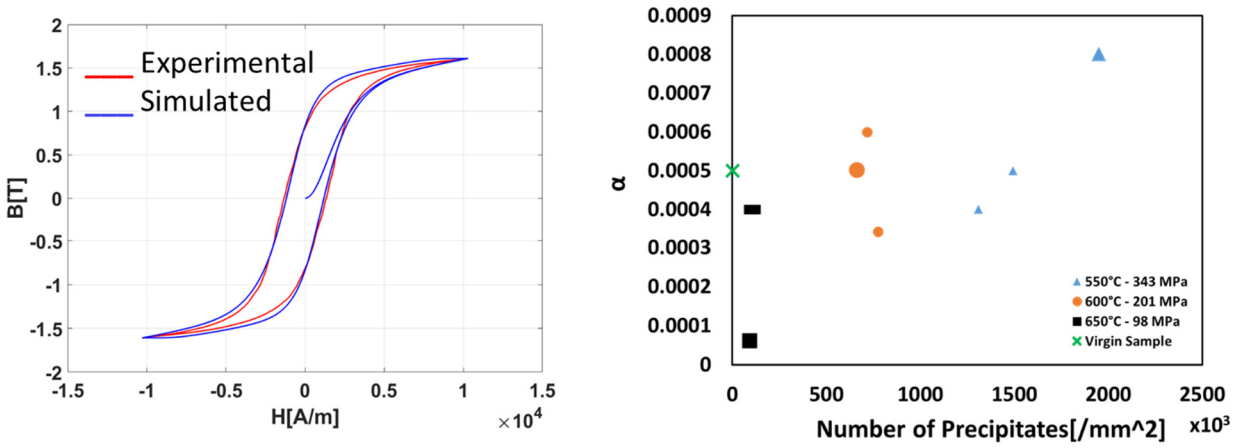

Figure 8: Comparison simulation/measurement and evolution of α simulation parameter as a function of number of precipitates.

As a first simulation result, Fig. 8 compares the simulated and experimental data for the virgin sample B(H) curve. Correlations between the simulation parameters and the microstructural properties can be established and observed as illustrated here.

3.2 Magnetic Barkhausen noise simulation

The motivation behind this simulation study was to derive a reliable parameter or a combination of parameters that could be used to interpret the material microstructure. As explained previously, the J–A model has been developed to simulate the hysteretic behavior of the ferromagnetic materials. The model has never been used to simulate the stochastic comportment of the magnetic Barkhausen noise raw signal and is not designed to do so. However, using an analogy, the model can be set to simulate the hysteresis behavior of other hysteretic situations of completely different natures (ferroelectricity [42]) and can even be used to simulate the MBN_{energy} hysteresis cycle [27].

To simulate the MBN_{energy} hysteresis cycle, this process starts by approximating the experimental MBN_{energy} anhysteretic curve. For this curve, we opted for a numerical estimation instead of experimental measurements because the experimental procedure is hazardous and for almost all classic soft magnetic materials, no large differences can be observed between the estimated and the measured anhysteretic curves. If we assume that the major hysteresis cycle as perfectly symmetrical, the MBN_{energy} anhysteretic curve can be calculated by using the increasing part of the cycle and Eq. (11).

$$H_i^{anhyst}(B_i) = \frac{H_i^{inc}(B_i) + H_i^{dec}(B_i)}{2} \qquad (10)$$

H_i^{inc} represents the *H* values for the increasing part of the major hysteresis cycle and H_i^{anhyst} represents the anhysteretic one. *Ms* and *a* are the J–A anhysteretic parameters that are calculated after fitting the estimated anhysteretic curve to the simulated one using the Matlab™ curve-fitting toolbox. An optimization code that is based on a minimization of an error function (Eq. 6.4) is run to evaluate the optimized α, k and c combination.

$$dH/dt > 0, \qquad H \in [H_{\min}, H_{\max}]$$
$$Error = \sum_{i=1}^{n} abs\left(\left|MBN_{energy}\right|_i^{\exp}(H_i) - \left|MBN_{energy}\right|_i^{sim}(Hi)\right) \tag{10}$$

Fig. 9 compares the simulated and measured data for the MBN_{energy} curves for one of the samples, and k parameter from the simulated curves for all samples with respect to the number of precipitates.

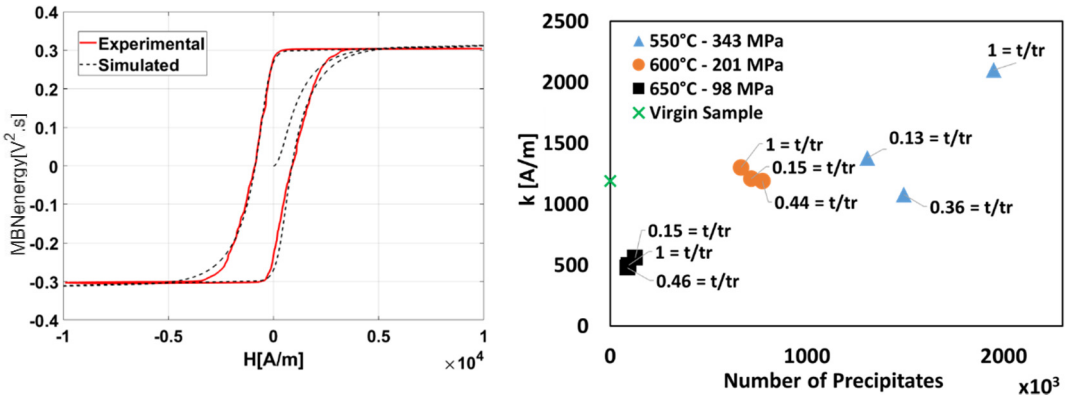

Figure 9: $MBN_{energy}(H)$ hysteresis cycles, k as a function of the number of precipitates.

3.3 Magnetic incremental permeability simulation

MIP simulation is a challenging task because it involves dealing and simulating minor loops that result from an alternating-current (AC)-superimposed direct-current (DC) magnetic field during magnetization and demagnetization [43][44]. From recent work on this scientific topic, Y. Gabi [45] implemented in the FEM FLUX software in order to describe the magnetic behavior of dual phase materials. A new computation strategy was developed and validated in 2D, separating the high frequency and the low frequency excitation contributions. L. Arbenz et al. [46] performed MIP to control a ferromagnetic plate, the four needles technique is used and just like in [45] an FEM simulation is proposed to simulate this experimental situation. D'aquino et al. [47] considered a whole single sheet tester that is spatially discretized and

simulated, the Jiles-Atherton model in its vector form is used for the local hysteresis consideration. Finally, Y. Gabi et al. [48] tested and simulated a yoke probe head and a pancake-type sensors. A 3D dynamic vector model is developed and gives correct simulation results for the incremental and differential permeabilities. In a conventional approach, to consider the magnetic field's distinct axial components and to simulate the inhomogeneous distribution of the magnetic field, a full 3D magnetic model is required. Alternatively, by assuming the magnetic flux B and applied magnetic field strength H are collinear, a simplified scalar analytical model can be used as shown in Fig. 10.

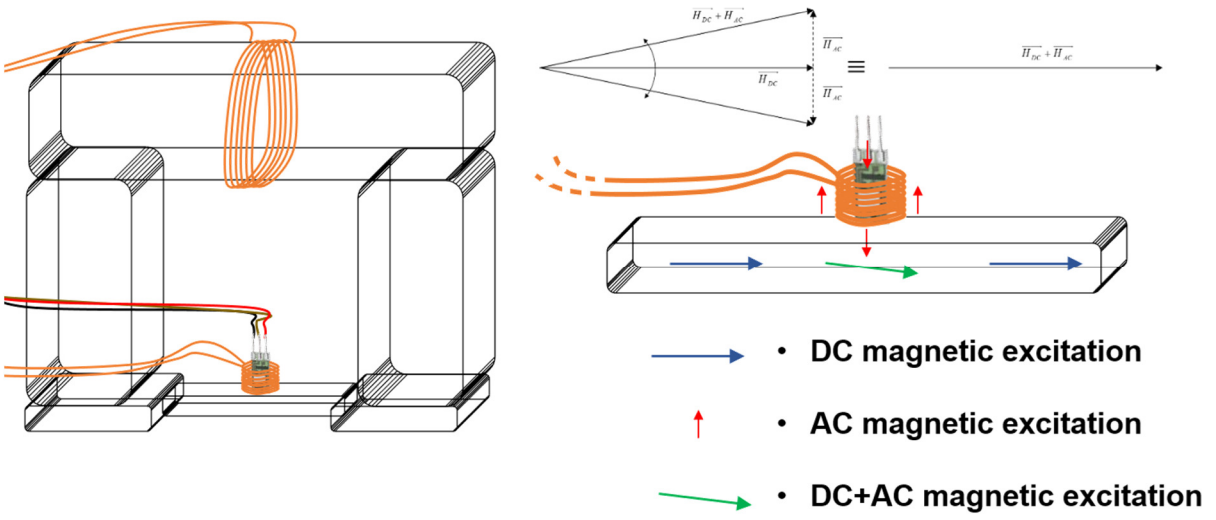

Figure 10: Overall 3D scheme of MIP experimental situation.

In the standard MIP experimental setup, AC and quasi-static (DC) magnetic excitations are vectorially perpendicular quantities. However, the maximum amplitude of the quasi-static magnetic excitation field tends to be one-thousand times the AC magnetic excitation field. Hence, during the larger part of the quasi-static magnetizing process, the orientation of the cumulative vector excitation field $\vec{H}(\overrightarrow{H_{DC}}+\overrightarrow{H_{AC}}$ contribution) remains nearly constant. As per this observation and to simplify the modelling scheme, the vector is considered to be collinear to $\vec{B}$ vector (induction). Based on this assumption, a scalar approach is considered to simulate

the material magnetic behavior, with the accurate scalar hysteretic material law. Additionally, the induced magnetization behavior becomes distributed homogeneously in the materials under investigation, when operating at a low H_{DC} frequency. Because the AC component has a small amplitude, the permeability is assumed to be nearly constant, which results in a direct proportionality between the measured output voltage amplitude and the permeability. Even at 50 kHz, the local excitation slope dH/dt as a result of the AC component is much lower than the maximum amplitude of dH/dt observed below the quasi-static field threshold. When the AC dynamic contribution is considered during minor loop conditions, it affects the phase shift among B and H but it still has an insignificant influence on the MIP signal (permeability modulus). As a result, the dynamic contributions are not considered in the following simulations. In this study, the focus is entirely on modelling the variations in permeability modulus against the applied magnetic field, which results in the so-called MIP butterfly loop. Because the objective is the simulation of the typical butterfly loop $|\mu|(H)$, it is sufficient to achieve good simulations considering only the quasi-static contribution. The J–A model has to be modified to address the accommodation issue (i.e., it requires multiple cycles to stabilize the minor hysteresis loops), which is resolved by considering that the AC component amplitude is sufficiently weak to neglect the hysteresis phenomena during the minor loop conditions. Fig. 11 compares the simulated and measured data for the MIP curves for one of the samples, and c parameter from the simulated curves for all samples with respect to the number of precipitates.

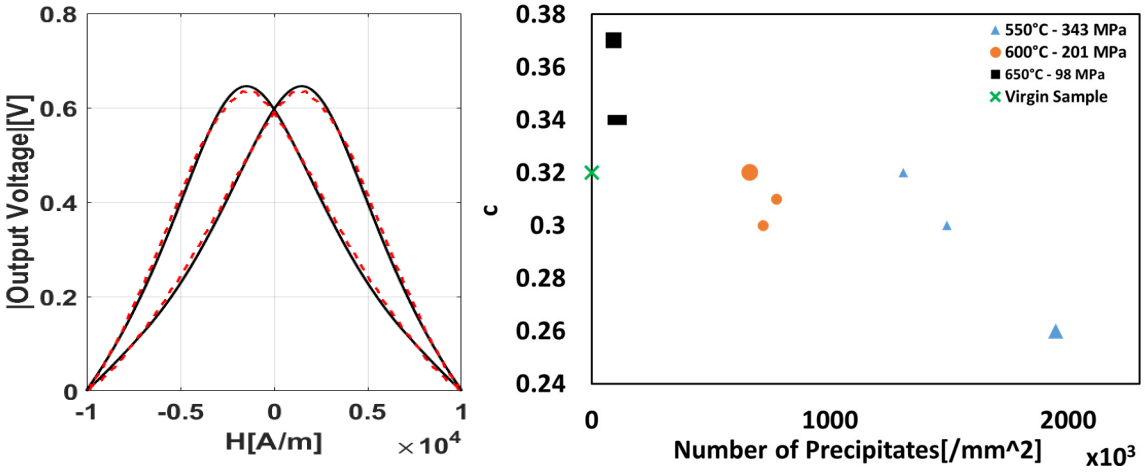

Figure 11: MIP(H) hysteresis cycles, c as a function of the number of precipitates.

Please note that even if the electrical conductivity has a strong influence on all the experimental situations tested in this study, it does not appear as a direct simulation parameter since it is considered as homogeneous over the sample geometry.

4 Correlations and observations

A correlation of the NDT signals with the microstructural information will help to provide tentative information on the material's state, by studying the NDT signals with time during the material lifecycle. Three different electromagnetic techniques were used to investigate the high-chromium ferritic creep test samples that were subjected to different temperature and stress conditions. In the derivation of magnetic signatures, this information is used to interpret the microstructure, which avoids the potential use of imaging techniques. A modelling technique has been developed to simulate the magnetic signatures that provide access to modelling parameters. These modelling parameters are correlated to the microstructure to reveal sensitivity information of each parameter with respect to each NDT technique used.

4.1 Conclusion from simulated results

The numerical approach that was proposed to simulate the three tested experimental situations in this study is based on the J–A model. The first simulation results from the B(H) cycles showed weak variations of the anhysteretic parameters *Ms* and *a*. Based on these observations, we decided to focus our correlation study on parameters α, k and c, which, according to J–A theory have a physical meaning that is related to the microstructure. α represents the inter-domain coupling, k is linked to the energy required to break the pinning site and c is linked to the reversible magnetization.

Prior to establishing the correlation with the microstructural observation and to creep, a parametric study based on an error function has been proposed to determine the level of sensitivity of the three parameters for the three experimental situations. The aim is to set a window for each parameter, to run every possible combination of parameters and to observe the evolution of the following error functions:

$$dH/dt > 0, \qquad H \in [H_{\min}, H_{\max}]$$

$$\begin{cases} Error_{B(H)} = \sum_{i=1}^{n} abs\left(\left|B\right|_i^{\exp}(H_i) - \left|B\right|_i^{sim}(Hi) \right) \\ Error_{MBN_{energy}} = \sum_{i=1}^{n} abs\left(\left|MBN_{energy}\right|_i^{\exp}(H_i) - \left|MBN_{energy}\right|_i^{sim}(Hi) \right) \\ Error_{MIP} = \sum_{i=1}^{n} abs\left(\left|\mu\right|_i^{\exp}(H_i) - \left|\mu\right|_i^{sim}(\mu) \right) \end{cases} \tag{10}$$

The results of this study are plotted in Fig. 12.

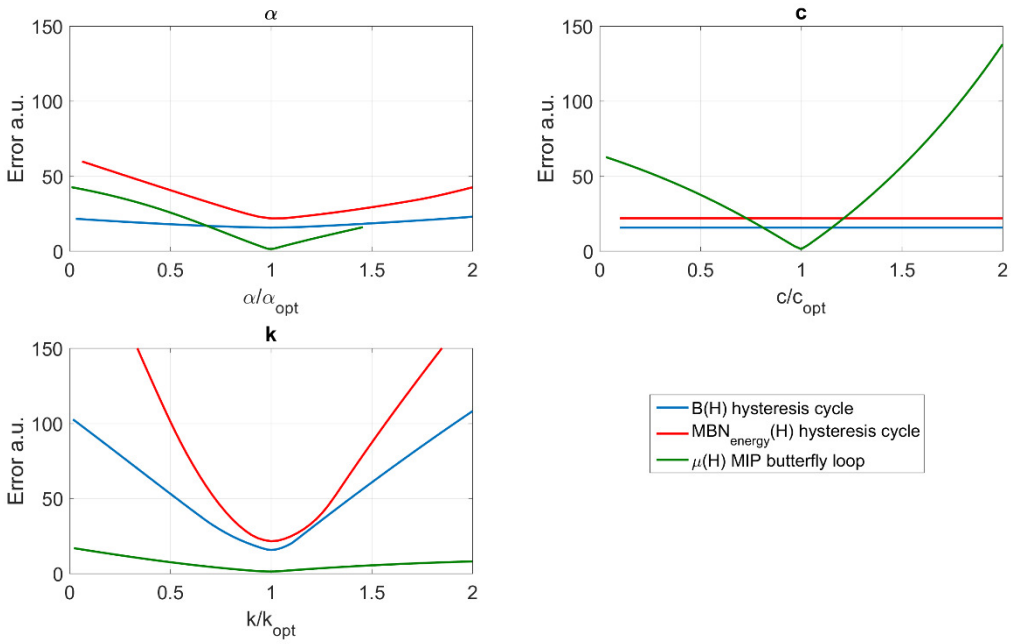

Figure 12: Simulation parameter sensitivity, based on error function.

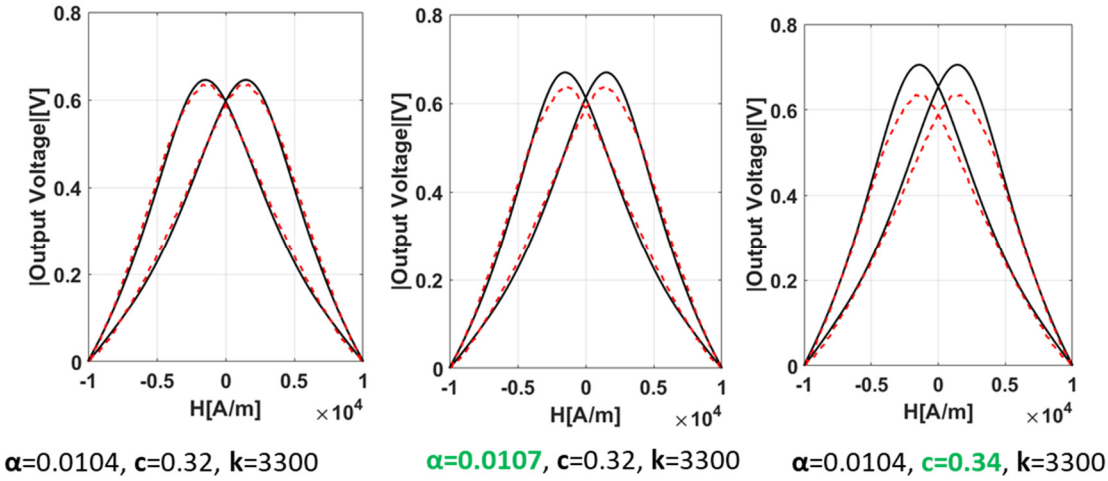

Figure 13: Simulation parameter sensitivity, based on error function, for MIP simulation.

These results have been obtained on the same sample, but the trends observed here are common to all ten samples tested, which means that the creep and aging history have no influence on the sensitivity of the simulation parameters. A flat variation of the error function

denotes a relative insensitivity of the simulation to the tested parameter. In contrast, a sharp variation means a strong influence.

α variations have a relatively weak influence on the B(H) simulations, which is not the case for the other two experimental situations. *k* is very sharp for the MBN_{energy} hysteresis cycle because the Barkhausen noise is connected strongly to the domain wall motion. *c* is flat for the B(H) and the MBN_{energy}(H) cycles and sharp for the MIP signature, which confirms the high influence of the reversible magnetization contribution to the butterfly loops. This study confirms the Barkhausen noise signature to observe domain wall motions and the magnetic incremental permeability for the magnetic reversible contribution or the inter-domain coupling. The result also shows the relatively weak sensitivity of the simulation parameters in a B(H) situation, where average information is supported and contributions cannot be separated.

With regards the link to the microstructural parameters in the B(H) simulations, α is higher for the lower-temperature treated samples, which supports the physics. The size of the precipitates (which may act as a pinning site between the domains) is much lower, which results in a higher inter-domain coupling. The modelling parameters and their evolution agree well with the magnetic parameter evolution that is obtained experimentally. Similar to the experimental results, the simulated hysteresis cycles do not show stronger variations between samples and this result is validated by the modelling parameters, because B(H) shows a good correlation factor only for one modelling parameter, i.e., α.

With regards a simulation of the MBN_{energy} hysteresis cycles, the *k* parameter that is associated with the coercivity shows a strong correlation with the microstructural properties of the materials.

The MIP simulation parameters show coherent trends because α is weak for the 650°C-treated samples where the precipitates are large and their number is weak, as is the domain interaction and the inter-domain coupling. For the 550°C-treated samples, the precipitates are smaller, this leads to high interactions between the domain walls and hence a higher α. The precipitates (which represent the carbide content) act mostly as a pinning site and are important in domain size expansion. A higher number of precipitates yields a larger precipitate area, and overall, more energy is required to break the pinning site. Therefore, *k*, is larger in lower-temperature-treated samples.

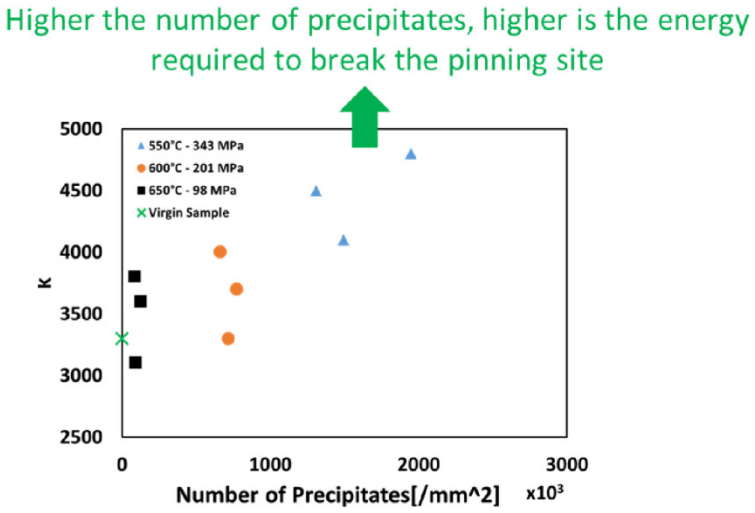

Figure 14: k as a function of the number of precipitates, in MIP situation

The crystal size in the higher-temperature treated samples is larger than the lower-temperature treated samples. Additionally, in the higher-temperature treated samples, the misorientation is lower. Therefore, the permeability of these samples would be higher and so would the magnetic reversibility, which is represented by *c* according to J–A theory and is illustrated in Fig. 15.

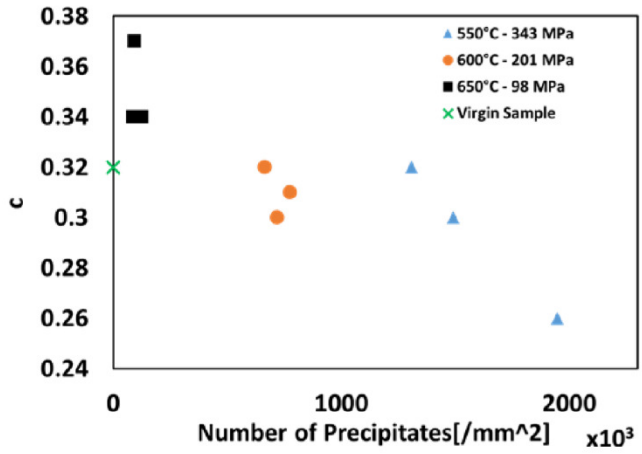

Figure 15: c as a function of the number of precipitates, in MIP situation

Experimentally, KAM does not show a good correlation with respect to magnetic parameters. Similarly, in the model-derived parameters, higher variations are observed only in higher-temperature samples. The 550°C-treated samples have a higher misorientation and dislocation than that of the higher-temperature samples, which means that a higher temperature provides the energy required to break the pinning site as illustrated in Fig. 16 (*k* parameter).

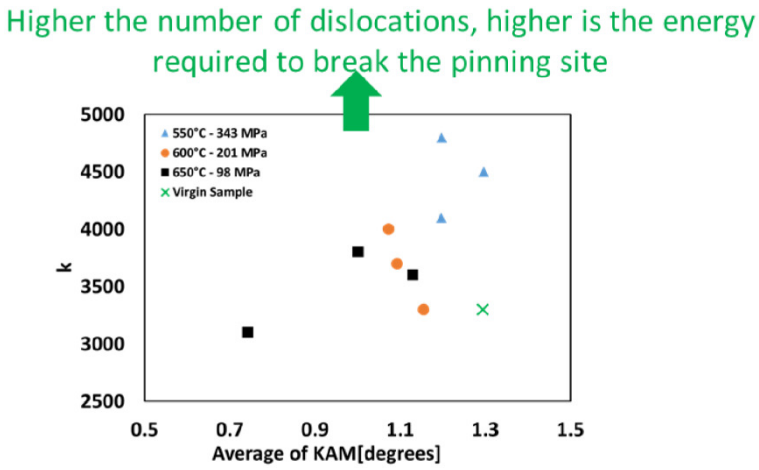

Figure 16: k as a function of KAM, in MIP situation

Because the higher-temperature treated samples have less misorientation, the magnetic reversibility would be higher as illustrated by the evolution of *c* in Fig. 17.

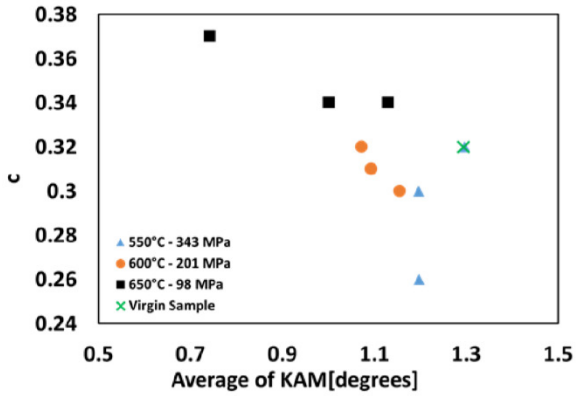

Figure 17: c as a function of KAM, in MIP situation

5 Conclusions

Large changes in the material microstructure of thermal power plant turbines and boilers occur with time because of constant exposure to high temperature and pressures. Even if imaging analysis provides quantitative microstructural data, the analysis cannot be performed during the controlled component lifecycle. Magnetic methods provide an alternative solution by delivering signals that are highly sensitive to microstructural changes in a nondestructive way.

In this study, three different magnetic signatures were tested to investigate high-chromium ferritic creep test samples that were subjected to different temperature and stress conditions. A derivation of magnetic signatures allowed for an interpretation of microstructure, which avoids the potential use of imaging techniques. Modelling techniques were developed to simulate the magnetic signatures and provide modelling parameters and physical interpretation. The modelling parameters were correlated with the microstructure, which revealed their sensitivity with respect to each NDT technique tested.

Strong correlations between the precipitation content and the incremental permeability parameters (cross-point, coercive field) were obvious. As has been demonstrated in the literature, grain misorientation analysis is a quantitative parameter to study creep. In this study, grain misorientation showed larger variations in high-temperature samples only. If the grain misorientation must be studied, the MIP coercive field tends to be the parameter used. Even if standard B(H) hysteresis cycles are the reference ferromagnetic characterization signatures, the sensitivity of this characterization method to microstructural changes is observable but limited because of geometric and magnetic response averaging and the natural filter process of this method because of the integration step. The magnetic Barkhausen noise, which depicts the domain wall speed, shows a good correlation in terms of microstructure evolution and hence can be used to predict the evolution of microstructural changes. Eventually, the amplitude of the MBN_{energy} curves decreases when rupture approaches.

The simulation results analysis leads to strong correlations. α, which is the inter-domain coupling, provides an example of where lower-temperature treated samples support the physics, because the precipitates (which may act as a pinning site between the domains) are smaller, and hence, a higher inter-domain coupling results. The *k* parameter, which is associated with the energy required to break pinning sites according to the J–A theory shows strong correlations with the precipitate number and size. This behavior is particularly true over the simulated B(H) coercive field and even more over the MIP field.

The ageing of the studied samples was extremely long, and the number of available samples was small. However, information was obtained on the nature, metallurgical treatments, and different sizes of the tested materials. The magnetic experimental and simulation conditions

can also be improved, because the final objective is to define the most sensitive magnetic factor.

The presence of chromium in the steel composition ensures the corrosion protection, however it creates inhomogeneity in the specimen physical properties (gradient of residual stress, deviation of the magnetic field ...). The magnetic behavior of the upper layers will definitively be different than the core ones. The penetration depth of the scanned area is different from one magnetic testing method to another. An estimation of these depths is clearly in the perspectives of this research project. We want to establish an accurate estimation of this penetration depth and from this to improve the comparison conclusion and to provide a better evaluation of each method performance.

References

[1] G. Sposito, C. Ward, P. Cawley, P.B. Nagy, C. Scruby, “A review of non-destructive techniques for the detection of creep damage in power plant steels”, NDT&E Int., Vol. 43, Iss. 7, pp. 555-567, 2010.

[2] F. Garofalo, “Fundamentals of creep and creep-rupture in metals”, Macmillan, New York, pp. 100, 1965.

[3] Y. Watanabe, “Materials aging damage and risk based maintenance”, 60st Shiraishi Memorial Lecture, Japan Iron & Steel Institute, Highly Information-Oriented Society and Steel Industry, Oct. 2008, Tokyo.

[4] K.W.J. Treadaway, “Studies of steel fracture by transmission and scanning electron microscopy, Building Research Station, Ministry of Public Building and Works”, Garston, Watford, Herts, Journal of Microscopy, Vol. 89, 2, 1969, pp. 283-286, 1969.

[5] M. Hussain, “Use or replication and portable hardness testing and high temperature plant integrity and life assessment”, Sem. Pow. & Proc. Plant Iss., Lahore, Pakistan, 2011.

[6] I. Tomas, O. Kovarik, G. Vertesy, J. Kadlecova, “Nondestructive indication of fatigue damage and residual lifetime in ferromagnetic construction materials”, vol. 25, 6, 065601, 2014.

[7] E. Du Trémolet de Lacheisserie, “Magnetism—Fundamentals, Materials and Applications”, Springer, Berlin, 2002.

[8] O. Hubert, L. Daniel, “Multiscale modeling of the magneto-mechanical behavior of grain-oriented silicon steels”, J. Magn. Magn. Mater., Vol. 320, pp. 1412-1422, 2008.

[9] B. Ducharne, MQ. Le, G. Sebald, P.J. Cottinet, D. Guyomar, Y. Hebrard, “Characterization and modeling of magnetic domain wall dynamics using reconstituted hysteresis loops from Barkhausen noise”, J. Magn. Magn. Mater., Vol. 432, pp. 231-238, 2017.

[10] Y. Mutoh, M.H. Attia, R.B. Waterhouse, “Improving fretting fatigue strength at elevated temperatures by shot peening in steam turbine steel, standardization of fretting fatigue test methods and equipment”, Eds., ASTM STP 1159. Philadelphia: American Society for Testing and Materials, pp. 119–209, 1992.

[11] B. Gupta, T. Uchimoto, B. Ducharne, G. Sebald, T. Miyazaki, T. Takagi, “Magnetic incremental permeability non-destructive evaluation of 12 Cr-Mo-W-V Steel creep test samples with varied ageing levels and thermal treatments”, NDT & E Int., Vol. 104, pp. 42-50, 2019.

[12] IEC 60404-3, “Methods of measurement of the magnetic properties of electrical steel strip and sheet by means of a single sheet tester”, Int. Electr. Com., 2002.

[13] ASTM A1036, “Guide for measuring power frequency magnetic properties of flat-rolled electrical steels using small single sheet testers”, ASTM International Tech. Rep., 2009.

[14] IEC 60404–2, “Magnetic materials Part 12: Guide to methods of assessment of temperature capability of interlaminar insulation coatings”, Int. Electr. Com., 1992.

[15] IEC 60404–4, “Methods of measurement of the magnetic dipole moment of a ferromagnetic material specimen by the withdrawal or rotation method”, Int. Electr. Com., 2002.

[16] P. Brissonneau, “Magnétisme et matériaux magnétiques”, Hermes, Science Publications, France, 1997.

[17] D.C. Jiles, “Review of magnetic methods for nondestructive evaluation”, NDT&E Int., Vol. 21, Iss. 5, pp. 311-319, 2003.

[18] S. Foner, “The vibrating sample magnetometer: experiences of a volunteer (invited)”, J. of App. Phys., Vol. 79, 4740, 1996.

[19] IEC 60404-2, "Magnetic materials – Part 2: Methods of measurement of the magnetic properties of electrical steel strip and sheet by means of an Epstein frame", Int. Elect. Com., June 2008.

[20] X. Kleber, A. Vincent, “On the role of residual internal stresses and dislocations on Barkhausen noise in plastically deformed steel”, NDT & E Int., Vol. 37, 6, pp. 439-445, 2004.

[21] A. Lasaosa, K. Gurruchaga, F. Arizti, “Induction hardened layer characterization and grinding burn detection by magnetic Barkheuse noise analysis”, J. of Nondestructive Ev., Vol. 36, 27, 2017.

[22] B. Ducharne, B. Gupta, Y. Hebrard, J.B. Coudert, “Phenomenological model of Barkhausen noise under mechanical and magnetic excitations”, IEEE Trans. on Mag, Vol. 99, pp. 1-6, 2018.

[23] O. Stupakov, J. Pal’a, T. Takagi, T. Uchimoto, “Governing conditions of repeatable Barkhausen noise response”, J. Magn. Magn. Mater., Vol. 231, 18, pp. 2956-2962, 2009.

[24] L. Piotrowski, B. Augustyniak, M. Chmielewski, E.V. Hristoforou, K. Kosmas, “Evaluation of Barkhausen noise and magnetoacoustric emission signals properties for plastically deformed armco iron”, IEEE. Trans. on Mag., Vol. 46, iss. 2, 2010.

[25] K. Gurruchaga, A. Martinez-de-guerenu, M. Soto, F. Arizti, “Magnetic Barkhausen noise for characterization of recovery and recrystallization”, IEEE. Trans. on Mag., Vol. 46, iss. 2, 2010.

[26] M. Soto, A. Martinez-de-guerenu, K. Gurruchaga, F. Arizti, “A completely configurable digital system for simultaneous measurements of hysteresis loops and Barkhausen noise”, IEEE. Trans. on Mag., Vol. 58, Iss. 5, 2009.

[27] B. Gupta, B. Ducharne, T. Uchimoto, G. Sebald, T. Miyazaki, T. Takagi, “Non-destructive testing on creep degraded 12% Cr-Mo-W-V ferritic test samples using Barkhausen noise”, J. Magn. Magn. Mater., Vol. 498, 166102, 2020.

[28] H. Chen, S. Xie, H. Zhou, Z. Chen, T. Uchimoto, T. Takagi, K. Yoshihara, “Numerical simulation of magnetic incremental permeability for ferromagnetic Material”, Int. J. App. Electromag. Mech., Vol. 45, pp. 379-386, 2014.

[29] T. Matsumoto, T. Uchimoto, T. Takagi, G. Dobmann, B. Ducharne, S. Oozono, H. Yuya, “Investigation of electromagnetic nondestructive evaluation of residual strain in low carbon steels using the eddy current magnetic signature (EC-MS) method”, J. Magn. Magn. Mater., Vol. 479, pp. 212-221, 2019.

[30] B. Gupta, B. Ducharne, T. Uchimoto, G. Sebald, T. Miyazaki, T. Takagi, “Physical Interpretation of the Microstructure for aged 12 Cr-Mo-V-W Steel Creep Test Samples based on Simulation of Magnetic Incremental Permeability”, J. Magn. Magn. Mater., Vol. 486, 165250, 2019.

[31] J.J. Lee, Y.K. Kim, S.H. Rhyu, I.S. Jung, S.H. Chai, J.P. Hong, “Hysteresis torque analysis of permanent magnet motors using Preisach model”, IEEE. Trans. on Mag., Vol. 48, iss. 2, 2012.

[32] Y. Saito, “Three-dimensional analysis of magnetodynamic fields in electromagnetic devices taken into account the dynamic hysteresis loops”, IEEE. Trans. on Mag., Vol. 18, iss. 2, 1982.

[33] M.A. Raulet, B. Ducharne, J.P. Masson, and G. Bayada, “The magnetic field diffusion equation including dynamic hysteresis: a linear formulation of the problem”, IEEE Trans. on Mag., Vol. 40, 2, pp. 872-875, 2004.

[34] B. Ducharne, D. Guyomar, G. Sebald, “Low frequency modelling of hysteresis behaviour and dielectric permittivity in ferroelectric ceramics under electric field”, J. of Phys. D: App. Phys., Vol. 40, 2, pp. 551-555, 2007.

[35] Y. Bernard, H. Maalej, L. Lebrun, B. Ducharne, “Preisach modelling of ferroelectric behavior”, Int. J. of App. Electromag. and Mech., Vol. 25, 1-4, pp. 729-733, 2007.

[36] F. Preisach, “Über die magnetische Nachwirkung”. Zeitschrift für Physik, Vol. 94, pp. 277-302, 1935.

[37] B. Zhang, B. Gupta, B. Ducharne, G. Sebald, T. Uchimoto, “Preisach’s model extended with dynamic fractional derivation contribution”, IEEE Trans. on Mag., Vol. 54, Iss. 3, 2017.

[38] A. Skarlatos, A. Martinez-de-guerenu, R. Miorelli, A. Lasaosa, C. Reboud, “A regressor-based hysteresis formulation for the magnetic characterization of low carbon steels”, Phys. B: Cond. Mat., vol. 581, 411935, 2019.

[39] D.C. Jiles, D.L. Atherton, “Theory of ferromagnetic hysteresis”. J. App. Phys., vol. 55, 2115, 1984.

[40] B. Zhang, B. Gupta, B. Ducharne, G. Sebald, T. Uchimoto, “Dynamic magnetic scalar hysteresis lump model, based on Jiles-Atherton quasi-static hysteresis model extended with dynamic fractional derivative contribution”, IEEE Trans. on Mag., Vol. 54, Iss. 11, pp. 1-5, 2018.

[41] D.C. Jiles, D.L. Atherton, “Ferromagnetic hysteresis”. IEEE Trans. on Mag., Vol. 19, Iss. 5, pp. 2183-2185, 1983.

[42] Y. Bai, B. Ducharne, H. Jantunen, J. Juuti, “Simulation and validation of temperature-dependent ferroelectric properties of multifunctional BCZT and KNBNNO ceramics”, Materials Research Express, Vol. 5, 116305, 2018.

[43] B. Wolter, Y. Gabi, C. Conrad, “Nondestructive testing with 3MA – An overview of principles and applications”, App. Sci., vol. 9, iss. 1068, 2019.

[44] Y. Gabi, D. Böttger, B. Straß, B. Wolter, C. Conrad, F. Leinenbach, “local electromagnetic investigations on electrical steel FeSi 3% via 3MA micromagnetic NDT system”, in Proceedings of the 12th European Conference on Nondestructive Testing, ECNDT 2018, Gothenburg, Sweden, 11–15 June 2018.

[45] Y. Gabi, « Modélisation FEM du Système de Contrôle non Destructif 3MA en Ligne de Production des Aciers Dual Phase », Ph.D. Thesis, Grenoble University, Grenoble, France, 2012.

[46] L. Arbenz, A. Benabou, S. Clénet, J.C. Mipo, P. Faverolle, “Characterization of the local incremental permeability of a ferromagnetic plate based on a four needles technique”, IEEE Trans. on Mag., vol. 53, iss. 3, pp. 1-7, 2017.

[47] M. D’aquino, S. Minucci, C. Petrarca, G. Rubinacci, A. Tamburrino, S. Ventre, “Micromagnetic measurements of ferromagnetic materials: Validation of a 3D numerical model”, NDT&E Int., vol. 104, pp. 77-89, 2019.

[48] Y. Gabi, K. Jacob, C. Wolter, B. Conrad, S. Strass, J. Grimm, “Analysis of incremental and differential permeability in NDT via 3D-simulation and experiment”, J. of Mag. and Mag. Mat., vol. 505, 166695, 2020.